Low Band Gap Polymer Solar Cells With Minimal Voltage Losses

Chuanfei Wang, Xiaofeng Xu, Wei Zhang, Jonas Bergqvist, Yuxin Xia, Xiangyi Meng, Kim Bini, Wei Ma,* Arkady Yartsev, Koen Vandewal, Mats R. Andersson, Olle Inganäs, Mats Fahlman, and Ergang Wang**

One of the factors limiting the performance of organic solar cells (OSCs) is their large energy losses (E_{loss}) in the conversion from photons to electrons, typically believed to be around 0.6 eV and often higher than those of inorganic solar cells. In this work, a novel low band gap polymer PIDTT-TID with a optical gap of 1.49 eV is synthesized and used as the donor combined with $PC_{71}BM$ in solar cells. These solar cells attain a good power conversion efficiency of 6.7% with a high open-circuit voltage of 1.0 V, leading to the E_{loss} as low as 0.49 eV. A systematic study indicates that the driving force in this donor and acceptor system is sufficient for charge generation with the low E_{loss}. This work pushes the minimal E_{loss} of OSCs down to 0.49 eV, approaching the values of some inorganic and hybrid solar cells. It indicates the potential for further enhancement of the performance of OSCs by improving their V_{oc} since the E_{loss} can be minimized.

1. Introduction

The advantages of light-weight, flexibility, and possibility for being semi-transparent, make polymer solar cells (PSCs) a promising photovoltaic technology. In recent decades, tremendous research efforts have pushed the power conversion efficiencies (PCEs) over 11% in polymers:fullerenes (e.g., PCBM) bulk-heterojunction solar cells.[1] However, PCEs of PSCs are still far behind those of inorganic counterparts, such as sc-Si, GaAs, CdTe, CIGS, and Perovskite solar cells.[2] One of the main reasons is their low open-circuit voltage (V_{oc}) due to the large energy loss per absorbed photon. The minimum energy loss (E_{loss}) is defined by the equation: $E_{loss} = E_g - qV_{oc}$, where E_g is the optical gap of the main light absorber, in most cases the donor material. Decreasing E_{loss} will enhance the V_{oc} and thus PCEs of PSCs.[3–5] The minimum E_{loss} for efficient charge generation in organic solar cells (OSCs) is suggested to be 0.6 eV,[6] and E_{loss} below 0.6 eV often leads to inefficient charge generation and low quantum efficiency, limiting the photocurrent and PCEs.[7] Typically, the E_{loss} for polymer:fullerene based PSCs with high PCEs of 9%–11% is between 0.7 and 0.9 eV.[8–10] In contrast, Perovskite solar cells have a high V_{oc} (> 1 V) with E_{loss} of ≈0.5 eV, which partially accounts for their much higher PCEs of ≈20%.[11,12] The E_{loss} values for inorganic solar cells, such as sc-Si, GaAs, GaInP, CdTe, CIGS-based solar cells are normally between 0.3 and 0.6 eV.[13] In **Figure 1** and Table S1 in the Supporting Information, we summarize a selection of solar cells exhibiting either

C. Wang, Prof. M. Fahlman
Division of Surface Physics and Chemistry
IFM
Linköping University
SE-581 83 Linköping, Sweden

Dr. X. Xu, K. Bini, Dr. E. Wang
Department of Chemistry and Chemical Engineering
Chalmers University of Technology
SE-412 96 Göteborg, Sweden
E-mail: xixu@chalmers.se; ergang@chalmers.se

Dr. W. Zhang, Dr. A. Yartsev
Division of Chemical Physics
Lund University
Box 124, 221 00 Lund, Sweden

Dr. J. Bergqvist, Y. Xia, Prof. O. Inganäs
Biomolecular and Organic Electronics
IFM
Linköping University
SE-581 83 Linköping, Sweden

X. Meng, Prof. W. Ma
State Key Laboratory for Mechanical
Behavior of Materials
Xi'an Jiaotong University
Xi'an 710049, China
E-mail: msewma@mail.xjtu.edu.cn

Prof. K. Vandewal
Institut für Angewandte Photophysik
Technische Universität Dresden
01069 Dresden, Germany

Prof. M. R. Andersson
Future Industries Institute
University of South Australia
Mawson Lakes Boulevard, Mawson, Lakes, SA 5095, Australia

DOI: 10.1002/aenm.201600148

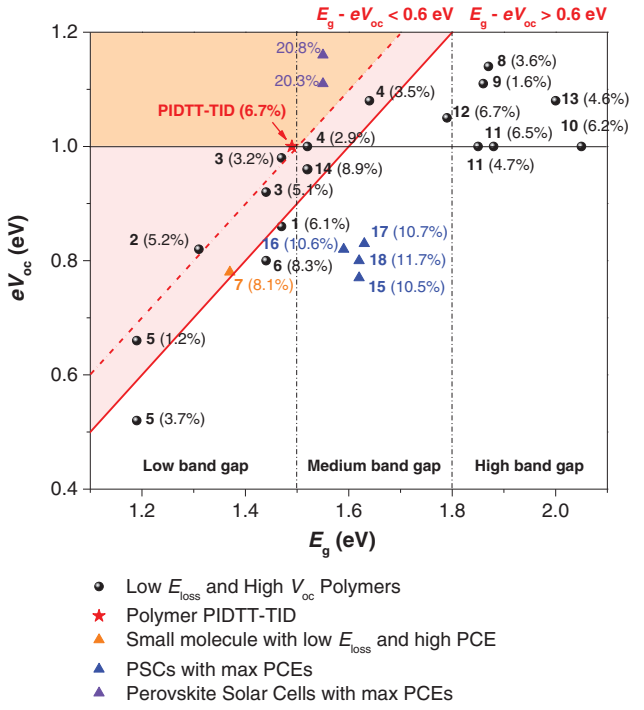

Figure 1. Plots of eV_{oc} against E_g for Perovskite and organic solar cells with low E_{loss} or high V_{oc}. E_g is determined from the absorption onset. The black solid line is the eV_{oc} of 1.0 eV, the red dashed line is the $eV_{oc} = E_g - 0.5$, and the red solid line is the $eV_{oc} = E_g - 0.6$. The PCEs are shown in the parentheses. The number of the points corresponds to the structures and device parameters listed in Table S1 in the Supporting Information.

low E_{loss} or high V_{oc}. Only few of the medium and low band gap polymers are located in the low E_{loss} area below 0.6 eV (on the left side of the red solid line).[4,5,14] A very recent report shows that only one of low band gap polymers (point 14 in Figure 1) attains a PCE of 8.9% with the E_{loss} below 0.6 eV.[15] A high V_{oc} above 0.8 V and PCE over 6% are still rarely observed among low band gap small molecules (point 7, Figure 1) and polymers (points 1 and 14 in Figure 1).[3,5] To date, molecular design rules dictating structural factors allowing for a lower E_{loss}, attaining both a high V_{oc} and high quantum efficiency are unclear. Moreover, the minimum E_{loss}, still enabling efficient free carrier generation and collection in OSCs is unknown. Therefore, it is highly important to conduct a systematic study to understand the minimization of E_{loss}.

In this contribution, we report a novel polymer poly[indacenodithieno[3,2-*b*]thiophene-*alt*-6-(2-ethylhexyl)-4,8-[1,2,5]thiadiazolo[3,4-*f*]isoindole-5,7-dione] (PIDTT-TID), which combines an electron-rich unit indacenodithieno[3,2-*b*]thiophene (IDTT) and an electron-deficient unit [1,2,5] thiadiazolo[3,4-*f*]isoindole-5,7-dione (TID). The rigid and planar structure of heptacyclic IDTT suppresses intramolecular rotation and enhances π-electron delocalization.[16,17] The TID unit is a strong electron-deficient moiety, combining the pyrrolodione and benzothiadiazole unit together. Very recent reports on several copolymers containing thiophene flanked TID acceptors have shown very low-lying the highest occupied molecular orbital (HOMO) and the lowest unoccupied molecular orbital (LUMO) levels.[18,19] Our design strategy for the polymer IDTT-TID is that, the combination of IDTT and TID units anchor the relatively deep HOMO and LUMO level to afford a low band gap polymer, potentially promoting a high V_{oc} and low-energy loss with sufficient driving force. Indeed, the polymer PIDTT-TID is characterized by a low E_g of 1.49 eV, and PSCs using PIDTT-TID as the donor (D) and $PC_{71}BM$ as the acceptor (A) provide a very high V_{oc} of 1.0 V and a PCE of 6.7%, which has rarely been reported among low band gap polymers. Interestingly, the E_{loss} ($E_g - qV_{oc}$) of the PSCs is only 0.49 eV, far less than the previously suggested minimum value of 0.6 eV.[6] This unique polymer shows that it is possible to design low band gap polymers with low E_{loss} but high V_{oc} and PCE for efficient PSCs. A set of experiments also demonstrate the extremely low E_{loss} but the existence of a sufficiently high driving force for free charge carrier generation in PIDTT-TID:$PC_{71}BM$ blends.

2. Results and Discussion

As depicted in Scheme S1 in the Supporting Information, the TID monomer was synthesized via a new procedure with moderate yields. The polymerization was carried out using Stille coupling of the stannylated monomer IDTT-*m* and brominated monomer TID (**Scheme 1**). The molecular weight was measured using size exclusion chromatography (SEC) at 150 °C and 1,2,4-trichlorobenzene as the eluent. The number-average molecular weight (M_n) of the polymer PIDTT-TID is 35.4 kDa with a polydispersity index of 3.7. The PIDTT-TID is readily soluble in chloroform and *o*-dichlorobenzene (*o*DCB) at high concentration (25 mg mL^{-1}) at room temperature.

Thermogravimetric analysis (TGA) shows that the temperature with 5% weight loss (T_d) of PIDTT-TID is as high as 455 °C, indicating the polymer has a high thermal stability (Figure S1a, Supporting Information). Differential scanning calorimetry (DSC) was used to investigate the phase transition and crystallization of the polymer. As shown in Figure S1b–e in the Supporting Information, there is no detectable thermal

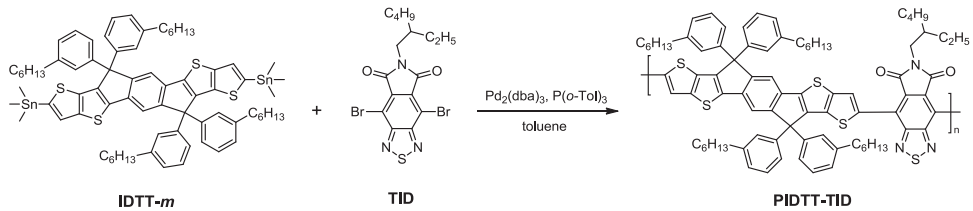

Scheme 1. Synthetic route of the polymer PIDTT-TID.

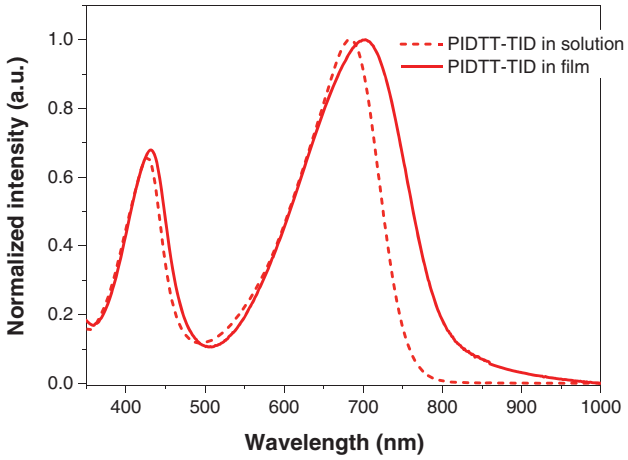

Figure 2. Normalized UV–vis–NIR absorption spectra of PIDTT-TID in *o*DCB and thin film.

transaction in the neat polymer and the blend films with D:A ratios from 1:2 to 1:4.

The normalized UV–vis–NIR absorption spectra of the polymer PIDTT-TID are shown in **Figure 2**. The absorption band in the wavelength range of 350–500 nm is attributed to a π–π^* transition, while a broader and red-shifted band in the wavelength range of 500–900 nm arises from the intramolecular charge transfer between the IDTT and TID moieties. A high absorption coefficient of 46.0 $Lg^{-1}cm^{-1}$ is recorded in *o*DCB solution (Figure S2a, Supporting Information). The absorption of the neat PIDTT-TID and PIDTT-TID:$PC_{71}BM$ blend films are shown in Figure S2b in the Supporting Information. Comparable absorption spectra are found between the measured UV–vis–NIR and those determined from the ellipsometry measurements. As shown in Figure S2c,d in the Supporting Information, a low E_g of 1.49 eV is determined from the onset of the optical absorption in the solid state, which is a commonly accepted and widely used method to determine optical gaps of conjugated polymers.[4,6,15,20–22] Another method is to derive this from the crossing of normalized UV absorption and emission spectra in the solid state, which gives a higher optical gap of 1.63 eV.[20] To compare with all of the E_g values from the literature we summarized in Figure 1, the E_g of 1.49 eV is used in this work.

Square-wave voltammetry (SWV) was used to determine the oxidation (E_{ox}) and reduction (E_{red}) potentials of PIDTT-TID and $PC_{71}BM$ (Figure S3, Supporting Information). PIDTT-TID and $PC_{71}BM$ feature HOMO levels of –5.89 and –6.44 eV, LUMO levels of –3.84 and –4.13 eV, respectively. Among IDTT-based polymers, this relatively deep HOMO level is a prerequisite for achieving a high V_{oc}. The offset between the LUMO levels of PIDTT-TID and $PC_{71}BM$ is 0.29 eV, which is close to the empirically determined but commonly accepted minimum value of 0.3 eV.[23]

To evaluate the photovoltaic performance of the polymer PIDTT-TID, solar cells with a device configuration of ITO/PEDOT:PSS/polymer:$PC_{71}BM$/LiF/Al were fabricated. The performance optimization consisted of varying the polymer:$PC_{71}BM$ weight ratios, active layer thicknesses, thermal annealing conditions, and solvent additives. A 25 mg mL^{-1} solution of PIDTT-TID and $PC_{71}BM$ in *o*DCB was found to be the optimal concentration, which provides the active layer thickness of 70–100 nm. The PSC parameters had no changes under gradual thermal annealing temperature at 80–150 °C for 10 min, implying that the corresponding PSCs have good thermal stability. The addition of solvent additive, such as 1,8-diiodooctane was found to have no positive effect on the device performance. The *J*–*V* curves are shown in **Figure 3**a. The PSC performance parameters (short-circuit current density J_{sc}, V_{oc}, fill factor FF, and PCE) are included in **Table 1**. For D:A ratios varying between 1:1 and 1:4, the PSCs consistently exhibit very high V_{oc} around 1.0 V, which is the highest V_{oc} among IDTT-based polymers.[16,24] It is especially rare to find such a high V_{oc} for a low band gap polymer with E_g below 1.5 eV. Besides a high V_{oc}, the polymer PIDTT-TID enables a good PCE of 6.7% with a J_{sc} around 12 mA cm^{-2} and FF above 0.5. The PSC parameters remain high over a large variation of D:A ratios from 1:2.5 to 1:4. External quantum efficiencies (EQE) were measured to evaluate the spectral response of the PSCs. As shown in Figure 3b, the EQE curves are consistent with the absorption spectra of PIDTT-TID:$PC_{71}BM$ blend films in the 400–900 nm region. The enhanced quantum efficiency in the region of 450–550 nm is attributed to the increasing content of $PC_{71}BM$ in the blends.

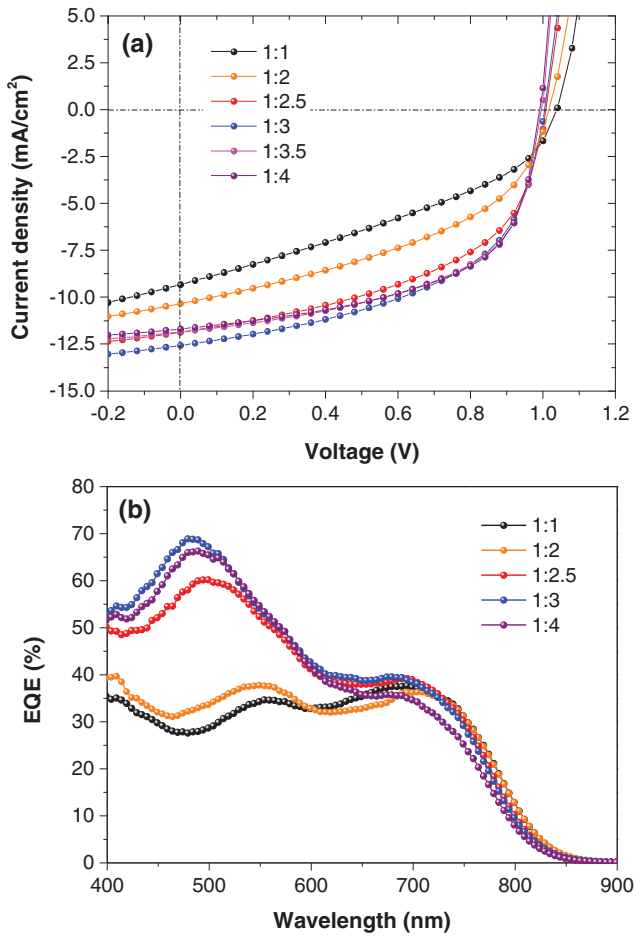

Figure 3. a) *J*–*V* characteristics and b) EQE profiles of the PIDTT-TID:$PC_{71}BM$ solar cells with different D:A ratios.

Table 1. Device parameters of the optimized PIDTT-TID:$PC_{71}BM$ solar cells.

Ratio[a)]	V_{oc} [V]	J_{sc} [mA cm^{-2}]	FF	PCE [%]	Hole mobility [cm^2 V^{-1} s^{-1}]
1:1	1.04	9.3	0.37	3.6	8.0×10^{-6}
1:2	1.01	10.5	0.45	4.8	6.4×10^{-6}
1:2.5	1.01	11.9	0.51	6.1	–
1:3	1.00	12.6	0.53	6.7	4.0×10^{-6}
1:3.5	1.00	11.9	0.56	6.7	–
1:4	0.99	11.7	0.57	6.6	5.2×10^{-6}

[a)]Polymer:$PC_{71}BM$ weight ratio.

The charge carrier mobility of the blend film is closely connected to its photovoltaic performance. The hole mobilities (μ_h) of the blend films were measured using the space charge limited current (SCLC) method. The current density and voltage (J–V) characteristics of hole only devices are shown in Figure S4 in the Supporting Information. The hole mobilities of the PIDTT-TID:$PC_{71}BM$ blends at different D:A ratios are within the same order of magnitude, ranging from 4.0×10^{-6} cm^2 V^{-1} s^{-1} to 8.0×10^{-6} cm^2 V^{-1} s^{-1}. The neat PIDTT-TID film shows the highest hole mobility of 9.6×10^{-6} cm^2 V^{-1} s^{-1}. Generally, the SCLC hole mobilities of IDTT-based copolymer:$PC_{71}BM$ are among 10^{-3} cm^2 V^{-1} s^{-1} and 10^{-4} cm^2 V^{-1} s^{-1}.[16,24,25] The hole mobilities measured in the PIDTT-TID:$PC_{71}BM$ blends are on the low side. This is probably due to the incorporation of bulky phenyl side chains on IDTT units, which can lead to reduced π–π stacking and amorphous property. This is confirmed by the DSC measurements and the morphology study on the PIDTT-TID:$PC_{71}BM$ blends in the next section, as there are no fiber-like crystals or preferential molecular orientation. This limits the charge carrier transport and leads to relatively low hole mobilities on the level of 10^{-6} cm^2 V^{-1} s^{-1}. Since the photocurrent and FF is highly dependent on efficient charge transport, the low mobilities can partially explain the modest J_{sc} and FF of the PIDTT-TID:$PC_{71}BM$ solar cells. Introduction of linear alkyl substituents, and functional groups with strong intermolecular interactions would enhance polymer orientation and morphological ordering in blend films, possibly increasing the μ_h, photocurrent, and FF.[26–28]

The morphology of active layers plays a key role in determination of their photovoltaic performance. To investigate the nanostructure of the blend films at different D:A ratios, a set of experiments including atomic force microscopy (AFM), transmission electron microscopy (TEM), grazing incidence wide-angle X-ray scattering (GIWAXS), and resonant soft X-ray scattering (RSoXS) were employed. AFM measurements depict the surface morphology of the blend films. As shown in **Figure 4** and Table S2 in the Supporting Information, for the D:A ratios of 1:1 and 1:2.5, each of the blend films forms a smooth surface with a small root-mean-square (RMS) roughness of 0.41 and 0.39, respectively. When the ratio of $PC_{71}BM$ increases from 1:3 to 1:4, the RMS roughness increases from 0.51 to 0.90 nm. TEM images show that when the ratio of $PC_{71}BM$ increases from 1:1 to 1:3.5, each of the blend film forms fine phase-separation with tiny (1–10 nm) $PC_{71}BM$ aggregates. For the ratio of 1:4, the dark areas are attributed to the $PC_{71}BM$-rich domains. For this stoichiometry, larger $PC_{71}BM$ aggregates appear but no big polymer domains are observed. On the basis of the AFM and TEM images, it is evident that the increasing content of $PC_{71}BM$, especially from 1:2.5 to 1:3.5, has a limited impact on the film morphology at the relevant length scale (≈10 nm), which is consistent with the comparable performance of PSCs at the large change of D:A ratios.

GIWAXS measurements were performed to depict the molecular orientation in the blend films. The 2D GIWAXS patterns and corresponding scattering profiles are shown in **Figure 5** and Figure S5a in the Supporting Information. All the (h00) scattering peaks are invisible, indicating an amorphous nature of PIDTT-TID, which is consistent with the DSC measurements. The similar in-plane and out-of-plane linecuts indicate the PIDTT-TID:$PC_{71}BM$ blends have no preferential orientation. As shown in Figure S5a in the Supporting Information, the neat PIDTT-TID film has a broad peak at $q \approx 1.43$ Å^{-1} (4.4 Å), which stems from the π–π stacking of polymer backbones. In

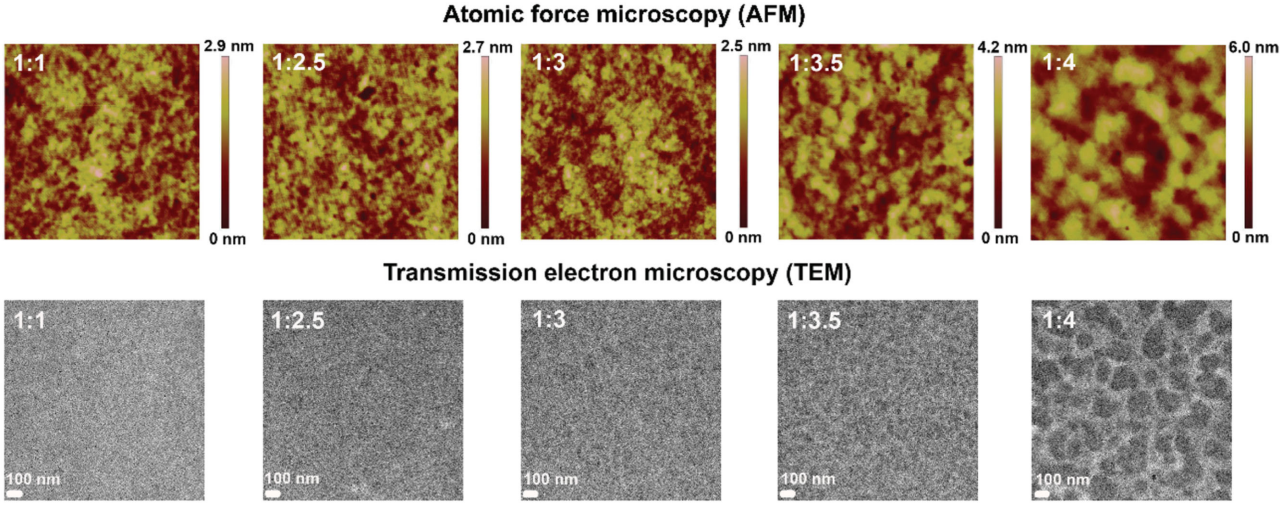

Figure 4. AFM topography (1 × 1 μm^2) and TEM bright field images (1.5 × 1.5 μm^2) of the PIDTT-TID:$PC_{71}BM$ blend films with different D:A ratios.

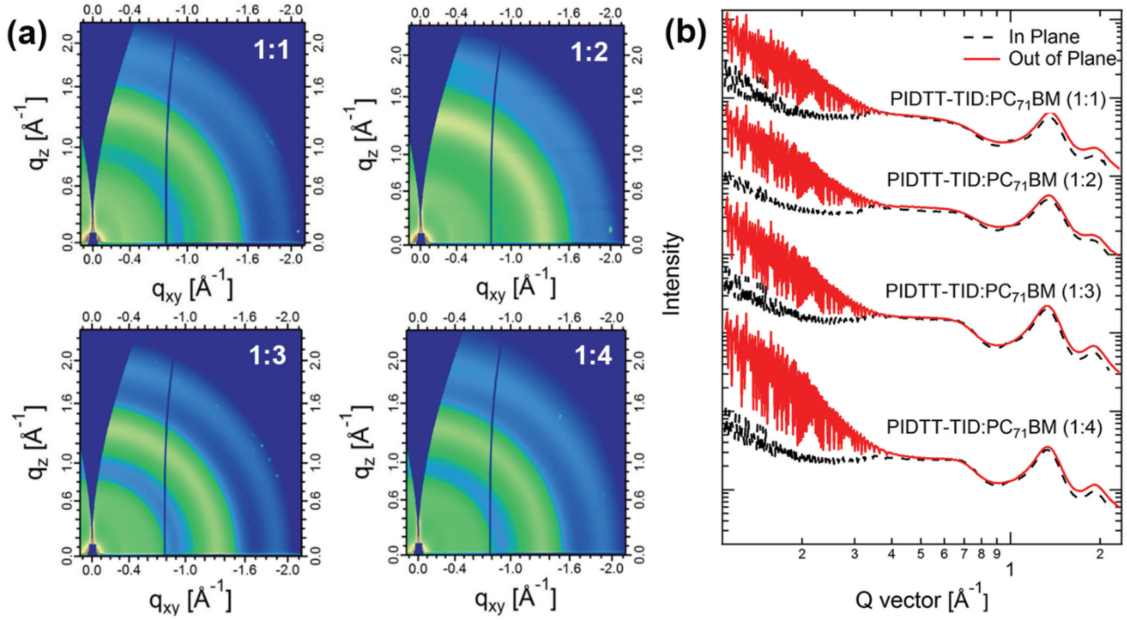

Figure 5. a) GIWAXS 2D patterns and b) scattering profiles of the PIDTT-TID:$PC_{71}BM$ blend films with different D:A ratios.

the neat $PC_{71}BM$ film, the broad and tiny peaks occurring at $q \approx 1.32$ Å^{-1} and 1.98 Å^{-1} corresponds to the $PC_{71}BM$ aggregates.[29] In the blend films, the PIDTT-TID and $PC_{71}BM$ reveal only one broad (010) peak at $q \approx 1.35$ Å^{-1}. In order to compare the π–π stacking characteristics of the PIDTT-TID, the (010) coherence length was revealed by the GIWAXS (010) peaks and calculated using the Scherrer equation. The (010) coherence length of the PIDTT-TID is 2.6, 2.8, 4.6, and 3.3 nm in the 1:1, 1:2, 1:3, and 1:4 blends, respectively. The highest coherence length is found in the 1:3 blend, indicating longer π–π stacking of the PIDTT-TID backbones in the charge transport direction.[30]

RSoXS measurements were employed to probe the phase separation of the blend films.[31–34] The profiles were acquired at 284.2 eV to get highly enhanced materials contrast. The mode of the distribution of the scattering (s_{mode}) corresponds to the characteristic mode length scale (ξ) of the corresponding lognormal distribution in real space with $\xi = 1/s_{mode}$, a model-independent statistical quantity. Within a simple morphological model, the value of ξ reflects the median domain spacing, while the domain size is roughly equal to $\xi/2$. As shown in Figure S5b in the Supporting Information, for the D:A ratios of 1:1 and 1:2, the domain sizes are less than 10 nm on average. No obvious phase separation appears, indicating a good miscibility of the polymer and $PC_{71}BM$. On increasing the ratio of $PC_{71}BM$ to 1:3, the domain size increases to 10–40 nm on average. Since typical exciton diffusion lengths are ≈10 nm, this value is among the ideal phase scale for efficient charge separation.[35] Thus, it explains well that the PSC at this D:A ratio yields the highest J_{sc} and PCE. However, when the $PC_{71}BM$ content increases to 1:4, the larger polymer domains and $PC_{71}BM$ aggregates lead to an increased length scale around 40–50 nm on average. The same size of phase separation is also observed in the TEM image. In this case, the well-aggregated $PC_{71}BM$ phases stem from the extra content of $PC_{71}BM$, but a continuous, fine phase-segregated morphology of D:A structure is still maintained. Moreover, there is no very large polymer domain observed in the TEM image, which means excitons generated in the polymer phase may still easily diffuse to the D:A interface to dissociate. As a result, the 1:4 blend provides almost the same V_{oc}, a slightly lower J_{sc} due to the lower polymer content, and comparable FF due to well-defined network in $PC_{71}BM$ phase. Therefore, a similar PCE is observed to that of 1:3 ratio. Furthermore, the relative composition variation over the length scales probed (referred as relative domain purity) in a two-component blend can be revealed via calculating the total scattering intensity (TSI) of the RSoXS profiles. For polymer:$PC_{71}BM$ blends, the morphology may comprise three phases, the pure and aggregated donor phase, the pure $PC_{71}BM$ domains, and the mixed amorphous regions. Proper aggregation of both the polymer and $PC_{71}BM$ could provide an efficient pathway that can help the charges sweep out of the mixed regions.[29] The relative domain purity indicates the relative purity of one phase to another phase in the mixed amorphous regions. It is worth noting that the relative domain purity may have a "sweet spot" in different polymer:$PC_{71}BM$ blends. Too low or too high domain purity may lead to worse performance.[34] In our case, the relative domain purity of PIDTT-TID are 0.89, 0.94, 0.96, and 1 in the (1:1, 1:2, 1:3, 1:4) blends, respectively. The 1:3 blend with the relative purity of 0.96 shows the best performance. The GIWAXS and RSoXS measurements are consistent with the amorphous behavior and fine-phase separation of PIDTT-TID:$PC_{71}BM$ (1:2.5–1:4) blends, as indicated by the DSC, AFM, and TEM measurements.

As the E_{loss} in PIDTT-TID:$PC_{71}BM$ is unusually low, it is essential to consider whether the PIDTT-TID:$PC_{71}BM$ blends have enough driving force for efficient exciton dissociation. A too high driving force leads to a low V_{oc}, but insufficient driving force restricts exciton dissociation and results in low J_{sc}. Here, the driving force of the PIDTT-TID:$PC_{71}BM$ blends were studied by a set of experiments including photoluminescence

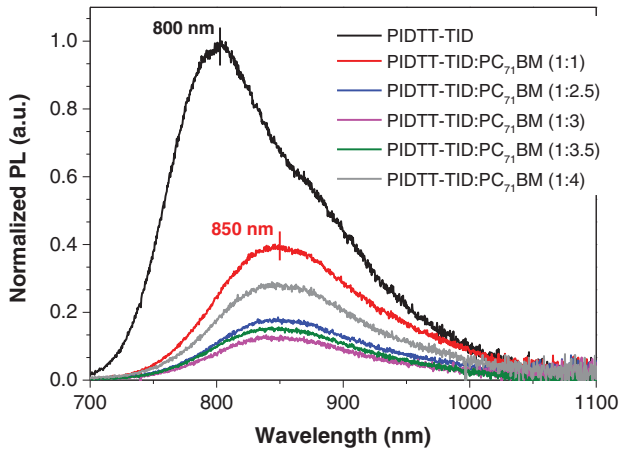

Figure 6. PL spectra of the neat PIDTT-TID and PIDTT-TID:$PC_{71}BM$ blend films with different D:A ratios.

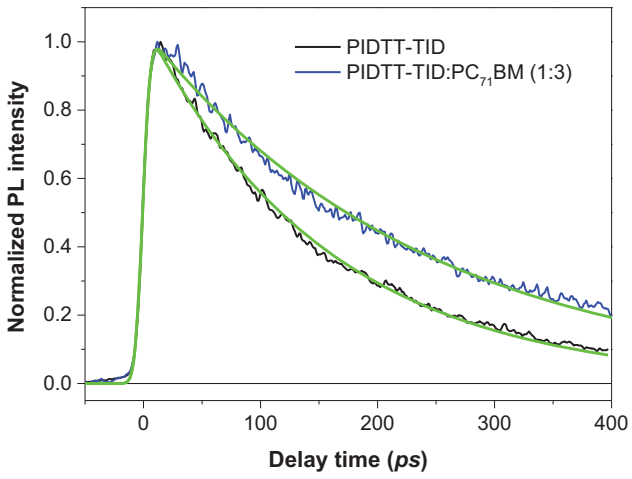

Figure 7. TRPL kinetics of the neat PIDTT-TID and PIDTT-TID:$PC_{71}BM$ (1:3) blend films under the same excitation power. Samples were excited at 400 nm, probing at 850 nm. Green lines are fitted curves based on the exponential functions.

(PL), time-resolved photoluminescence (TRPL), electroluminescence (EL), and charge transfer (CT) state absorption measurements. As shown in **Figure 6**, the emission of PIDTT-TID at 800 nm is fully quenched when it is blended with $PC_{71}BM$, due to the photo-induced CT.[36] This is the first indication of a sufficient driving force for charge transfer in the PIDTT-TID:$PC_{71}BM$ blends. Moreover, upon blending the appearance of a distinct peak at 850 nm is observed. Since the emission peak of $PC_{71}BM$ is around 720 nm, it does not originate from neat $PC_{71}BM$ emission.[37] To investigate the origin of this red-shifted emission, PL quenching measurements of the neat PIDTT-TID and PIDTT-TID:$PC_{71}BM$ blends were performed under reverse bias voltages (Figure S6, Supporting Information). In the blend films, we find a significant quenching of the emission upon the application of an electric field (reverse voltage), as opposed to the emission of the neat polymer. This suggests that the red-shifted emission at 850 nm most likely originates from the radiative decay of CT states at the interface between PIDTT-TID and $PC_{71}BM$.[38,39] Similar evidence for the presence of such CT states in polymer:PCBM and polymer:polymer blends has been presented previously.[40–42]

To study the charge photo-generation processes in PIDTT-TID:$PC_{71}BM$ films, we measured the TRPL kinetics of neat PIDTT-TID and PIDTT-TID:$PC_{71}BM$ blends. A pronounced excitation power dependence is recorded for the neat PIDTT-TID (Figure S7a, Supporting Information), which is attributed to enhanced exciton–exciton annihilation.[43,44] However, the decay dynamics of the PIDTT-TID:$PC_{71}BM$ blend (1:3) do not change notably under both low and high excitation power (Figure S7b, Supporting Information). Since the weak excitation power dependence is an important feature of the CT state, this result supports the assignment of CT emission in the blend films.[43,45] **Figure 7** and Figure S8 in the Supporting Information show the TRPL kinetics of the neat PIDTT-TID and PIDTT-TID:$PC_{71}BM$ blend films. We find that the time of CT formation is very fast (within the time resolution of 10 ps), and no slow formation processes was observed, indicating that polymer excitons are dissociated within 10 ps at the D:A interface. The efficiency of exciton dissociation in the blend film is calculated via the exciton lifetime in the neat PIDTT-TID and PIDTT-TID:$PC_{71}BM$ blend (1:3), and is higher than ≈90%. This shows that excitons dissociate efficiently in the PIDTT-TID:$PC_{71}BM$ blend. For the PIDTT-TID:$PC_{71}BM$ (1:3) blend film, we note that the PL lifetime of CT state is ≈230 ps, which is significantly longer than the exciton lifetime (≈156 ps) in the neat polymer. Since the CT state can dissociate into free carriers or recombine to ground state, a low CT state recombination rate facilitates CT state dissociation.[46,47] Moreover, since the emission of the PIDTT-TID:$PC_{71}BM$ blends stems from the CT state, in a simplified picture, the decay dynamics of the TRPL curves are related to the driving force. The rise of TRPL kinetics will, in its turn, depend on the degree of the singlet state (S1) dissociation. For example, if the driving force is insufficient, it would take a long time for the lowest lying S1 excitons to dissociate. In this case, a slow formation of the CT state from the S1 excitons should be seen in the TRPL curve.[48] However, as we mentioned above, the rate of CT state formation is very fast in the PIDTT-TID:$PC_{71}BM$ blends. This indicates that the driving force in these blends is enough for the CT state generation and exciton dissociation.

Additional proof for the presence of a sufficiently high driving force at the PIDTT-TID:$PC_{71}BM$ interface comes from the *J*–*V* characterization of PSCs under large reverse bias voltages (Figure S9, Supporting Information). Both of the light and dark current do not vary significantly for reverse bias voltages between 0 and −5 V. This implies that the driving force at the PIDTT-TID:$PC_{71}BM$ interface enables the excitons to dissociate into free charges which are eventually being collected at the electrodes. Furthermore, as shown in Figure S10a in the Supporting Information, compared to neat PIDTT-TID, a significant EL red shift occurs in the PIDTT-TID:$PC_{71}BM$ (1:3) blend due to the CT state emission. The offset between emission peaks of neat PIDTT-TID and the PIDTT-TID:$PC_{71}BM$ blend is proportional to the driving force for the exciton dissociation.

CT excitons are considered as weakly bound electron and hole pairs at the D:A interface, and crucial intermediates between the S1 exciton and free charge carriers. The energy of

the CT state (E_{CT}) is the effective band gap of a certain D–A pair. From the PL, TRPL, and EL measurements, the adjacent emitting peaks from the neat PIDTT-TID and its CT state suggest that the S1 state of the polymer with energy E_{S1} is close to the CT state with energy E_{CT}. Since the V_{oc} has been found to positively correlate with the E_{CT} in polymer:PCBM blends, the relatively high E_{CT} of the PIDTT-TID:$PC_{71}BM$ blend explains the very high V_{oc} in PIDTT-TID:$PC_{71}BM$ solar cells.[27,49] In an attempt to determine the value of the E_{CT} and the driving force (E_{S1}–E_{CT}), the EQE of the CT state absorption (EQE_{CT}) was measured using Fourier-transform photocurrent spectroscopy (FTPS) (Figure S10b, Supporting Information). Normally, the value of E_{CT} are obtained from a Gaussian fit to the CT band in the FTPS-EQE spectrum.[50] However, since the E_{CT} of the PIDTT-TID:$PC_{71}BM$ blend is close to the E_{S1} of the neat polymer, only a broad spectrum with no distinct shoulder of CT absorption was observed in the FTPS-EQE spectra for this particular blend, preventing an unambiguous fit.

In order to do more detailed study on energy losses, the energy losses ($E_{CT} - qV_{oc}$) in PSCs can be categorized in two types, energy losses due to radiative ($q\Delta V_{rad}$) and non-radiative ($q\Delta V_{nonrad}$) recombination, described by Equation (1).[51] For PSCs, additional energy losses are due to the differences between E_{CT} and optical gap E_{S1},[51] which in the case of PIDTT-TID:$PC_{71}BM$ is very small as we mention above. The radiative energy losses are in principle unavoidable, since any light absorber should also emit light. If caused by defects and impurities, non-radiative recombination is avoidable, resulting in a maximum V_{oc} if the electroluminescence external quantum efficiency (EQE_{EL}) is close to 1.[51] The PIDTT-TID:$PC_{71}BM$ blend shows an EQE_{EL} of 1.8×10^{-4} (Figure S11, Supporting Information), resulting in a ΔV_{nonrad} of 0.24 V via Equation (2), which is a very low value among OPV materials. Generally, the inorganic solar cells have the lowest ΔV_{nonrad} in the range of 0.04–0.21 V.[52] For Perovskite solar cells, it is around 0.2–0.5 V.[52] PSCs show higher ΔV_{nonrad} in the range 0.3–0.6 V.[51,52] The high-performance polymer PTB7 has a medium ΔV_{nonrad} of 0.39 V.[52] Therefore, the low $q\Delta V_{nonrad}$ contributes significantly to the low E_{loss} of the PIDTT-TID:$PC_{71}BM$ system. From the FTPS-EQE spectrum (Figure S10b, Supporting Information), the open-circuit voltage (V_{oc}^{rad}) when the radiative recombination is the sole loss mechanism can be calculated using the procedure described in literature.[50,52] For the PIDTT-TID:$PC_{71}BM$ (1:3) blend, we find a V_{oc}^{rad} around 1.24 V. Subtracting the ΔV_{nonrad} (0.24 V) from the V_{oc}^{rad} (1.24 V), we obtain a calculated V_{oc} of 1.0 V, which is exactly the same as the measured result.

$$V_{oc} = \frac{E_{CT}}{q} - \Delta V_{rad} - \Delta V_{nonrad} \quad (1)$$

$$\Delta V_{nonrad} = \frac{kT}{q} \ln\left(EQE_{EL}^{-1}\right) \quad (2)$$

In order to optimize the photovoltaic performance of the PIDTT-TID:$PC_{71}BM$ system, we also investigated the response of PIDTT-TID:$PC_{71}BM$ blends under different thicknesses. The maximum short-circuit photocurrent density ($J_{sc\text{-}max}$) as a function of the film thickness is shown in Figure S12 in the Supporting Information. The refractive index n and absorption coefficient k of PIDTT-TID:$PC_{71}BM$ blends were obtained via modelling the data from ellipsometry measurements. Assuming all the photons absorbed by the active layer are converted into the photocurrent, the maximum $J_{sc\text{-}max}$ is simulated by the transfer matrix model simulation. For the D:A ratio of 1:3, two photocurrent maxima are found at the range of 50–300 nm. The first photocurrent maximum is located at a thickness of around 90 nm, which is considered to be the optimized thickness of the active layer. The $J_{sc\text{-}max}$ calculated at the first photocurrent maximum is close to 15 mA cm^{-2}. As a comparison, the experimental J_{sc} is also included. The experimental J_{sc} is in a good agreement with the simulated $J_{sc\text{-}max}$ with an average of 84%. As illustrated in Figure S9 in the Supporting Information, when the J–V curve is swept to the high reverse voltage of –5 V, the experimental current approaches the simulated $J_{sc\text{-}max}$ of 15 mA cm^{-2}.

In theory, several empirical models determinate the maximum PCEs in a range of 10%–20% for single junction PSCs.[53] Synthesis of low band gap polymers is essential to achieve efficient solar energy harvest and high J_{sc}. However, the HOMO/LUMO levels of low band gap polymers and fullerenes should maintain the maximum V_{oc} and enough driving force for efficient exciton dissociation. Therefore, high-performance PSCs always require a comprehensive consideration. Among the low band gap polymers reported in the last decade, only few of them have both high V_{oc} and PCEs. As depicted in Figure 1, among the high V_{oc} polymers that are above 1.0 V (on top of the black solid line), only polymers 10, 11 and 12 based on benzo[1,2-*b*:4,5-*b*']dithiophene (BDT) and thieno[3,4-*c*]pyrrole-4,6-dione (TPD), show comparable PCEs around 6.5%, but the band gaps (1.8–2.0 eV) of the three polymers are much larger compared to the polymer PIDTT-TID.[54–56] For now, none of the small molecules or polymers with E_g below 1.5 eV attains a V_{oc} as high as 1 V. Very recently, Kazuo et al. reported a low band gap copolymer PNOz4T with E_g of 1.52 eV, which shows low E_{loss} of 0.52–0.56 eV (point 14 in Figure 1).[15] Upon blending with the $PC_{61}BM$ acceptor, PNOz4T showed a V_{oc} of 1 V and PCE of 5.6%. Increasing the content of $PC_{61}BM$ to 1:3, the V_{oc} slightly decreased to 0.97 V, and PCE was increased to 8.8%. Two other polymers (points 1 and 6 in Figure 1) and one porphyrin-based small molecule (point 7 in Figure 1) were reported with the E_g below 1.5 eV, while both points 6 and 7 attain V_{oc} around 0.8 V, PCEs above 8% and E_{loss} around 0.6 eV. The low band gap and large energy loss usually limit the value of V_{oc}, and very few high performance materials have been obtained from low band gap polymers.[57–59] In this work, the low band gap polymer PIDTT-TID shows a high V_{oc} of 1.0 V, PCE of 6.7%, and one of the lowest E_{loss} (0.49 eV) among photovoltaic polymers. We performed a set of measurements, which has proved that sufficient driving force exist for efficient exciton dissociation in the PIDTT-TID:$PC_{71}BM$ blends. This is a solid proof that a low band gap (<1.5 eV) polymer with such a low E_{loss} of 0.49 eV can attain enough driving force. As depicted by the blue points in Figure 1, the record-efficient polymers (points 15, 16, 17, and 18 in Figure 1) with PCEs over 10% show moderate V_{oc} around 0.8 V, medium E_g around 1.6 eV, and relatively high E_{loss} around 0.8 eV.[1,8,9,60] One of the efficient Perovskite solar cells shows a high V_{oc} of 1.09 V, narrow E_g around

1.6 eV, and low E_{loss} around 0.5 eV.[12,61] Very recently, a Perovskite solar cell attains a higher V_{oc} of 1.16 V, lower E_{loss} around 0.4 eV, and a PCE of 20.8% (purple point in Figure 1).[62] The PIDTT-TID:$PC_{71}BM$ system approaches the V_{oc} and E_{loss} of the high-performance Perovskite solar cells.

3. Conclusion

In conclusion, our work provides the synthesis and characterization of a new polymer PIDTT-TID, which incorporates alternating IDTT and TID units in the backbone. The polymer features a high molecular weight, a low band gap, deep HOMO, and LUMO levels. As a consequence, a PSC based on PIDTT-TID:$PC_{71}BM$ affords a high V_{oc} of 1.0 V, moderate photocurrent and FF, and a decent PCE of 6.7%. PIDTT-TID is one of the first low band gap polymers with E_g below 1.5 eV, which affords a high V_{oc} of 1.0 V and decent PCE over 6% at the same time. The good performance depends only slightly on the fullerene load without the necessity of additives and annealing, which makes it a robust system to produce and use. The high V_{oc} and J_{sc} correspond to its relatively high-energy CT state, while maintaining a sufficient driving force for charge dissociation. Of particular relevance for PSCs is the extremely low photo energy loss (E_{loss} = 0.49 eV) due to the very low non-radiative energy loss ($q\Delta V_{nonrad}$ = 0.24 eV), but enough driving force in the PIDTT-TID:$PC_{71}BM$ system. In addition, the V_{oc} and E_{loss} of the PIDTT-TID:$PC_{71}BM$ solar cell is close to those of Perovskite solar cells. On-going studies will focus on how to achieve higher PCEs by improving mobility and morphological features by enhancing molecular orientation.

4. Experimental Section

Material Characterization: ^1H NMR (400 MHz) and ^{13}C NMR (100 MHz) spectra were measured on a Varian Inova 400 MHz NMR spectrometer with the tetramethylsilane as the internal reference. Matrix-assisted laser desorption ionization time of flight was performed on a Bruker Autoflex Speed spectrometer. SEC was carried out on an Agilent PL-GPC 220 Integrated High Temperature GPC/SEC System with refractive index and viscometer detectors. The columns were 3 PLgel 10 μm MIXED-B LS 300 × 7.5 mm columns. The eluent was 1,2,4-trichlorobenzene at 150 °C. The molecular weights were calculated according to relative calibration with polystyrene standards. TGA was carried out on a METTLER TOLEDO thermogravimetric analyzer TGA/DSC 3+, from 50 to 500 °C at a heating rate of 20 °C min^{-1} under N_2 flow. DSC was carried out on a METTLER TOLEDO differential scanning calorimeter DSC 2, from 0 to 300 °C at a heating and cooling rate of 10 °C min^{-1} under N_2 flow. UV–vis–NIR absorption spectra were measured with a Perkin Elmer Lambda 900 UV–vis–NIR absorption spectrometer. A RC2 instrument (J.A. Woolam Co., Inc.) was used to perform variable angle spectroscopic ellipsometry (VASE) measurements with the incident angles being varied from 45° to 75° in steps of 10° on the prepared thin films. The modelling of VASE measurement was performed by using the software Complete Ease (J.A. Woolam Co., Inc). Optical constants *n* and *k* were obtained by B-spline models. Samples were prepared from the *o*DCB solution of PIDTT-TID and PIDTT-TID:$PC_{71}BM$ (1:3) blend. Samples were spin-coated on clean silicon substrates with a 1 nm oxide layer. SWV measurements were carried out on a CH-Instruments 650A Electrochemical Workstation. A 0.1 M nitrogen-saturated solution of tetrabutylammonium hexafluorophosphate (Bu_4NPF_6) in anhydrous acetonitrile was used as the supporting electrolyte. Platinum wires were used for the working electrode and counter electrode. Ag/Ag^+ was used for the reference electrode. Potentials were referenced to the ferrocenium/ferrocene (Fe/Fe^+) couple by using ferrocene as an internal standard. Polymer films were deposited onto the working electrode from the chloroform solution. PL and EL spectra were taken with a Shamrock sr-303i-B spectrograph from Andor Tech., coupled to a Newton EMCCD Si array detector.

PSC Fabrication and Characterization: The structure of PSC was Glass/ITO/PEDOT:PSS/polymer:$PC_{71}BM$/LiF/Al. As a buffer layer, PEDOT:PSS (Baytron P VP Al 4083) was spin-coated onto ITO-coated glass substrates, followed by annealing at 150 °C for 15 min to remove the water. The thickness of the PEDOT:PSS layer was around 40 nm, as determined by a Dektak 6 M surface profilometer. The active layer, consisting of the PIDTT-TID:$PC_{71}BM$ blend, was spin-coated from *o*DCB solution onto the PEDOT:PSS layer. Spin coating was done in a glove box and active layers were directly transferred to a vapor deposition system mounted inside of the glove box. LiF (0.6 nm) and Al (100 nm) were used as the top electrodes, and deposited via a mask under vacuum onto the active layer. The accurate area of every device (4.6 mm^2) defined by the overlap of the ITO and Al electrode, was measured using a microscope. PCEs were calculated from the *J–V* characteristics recorded by a Keithley 2400 source meter under the illumination of an AM 1.5G solar simulator with an intensity of 100 mW cm^{-2} (Model SS-50A, Photo Emission Tech., Inc.). The light intensity was determined using a standard silicon photodiode. EQE profiles were measured by a Newport Merlin lock-in amplifier. The chopped monochromatic light (532 nm) was illuminated through an aperture of 2 mm on the transparent side.

Hole Mobility Characterization: Hole mobilities of the PIDTT-TID:$PC_{71}BM$ blend films were measured using the SCLC method. The structure of the hole-only device was ITO/PEDOT:PSS /polymer:$PC_{71}BM$/MoO_3/Al. The mobility was determined by fitting the dark current to the model of a single carrier SCLC, which was described by the equation:

$$J = \frac{9}{8}\varepsilon_0\varepsilon_r\mu_h\frac{V^2}{d^3}$$

where *J* was the current, μ_h was the charge mobility at zero field, ε_0 was the free-space permittivity, ε_r was the relative permittivity of the material, *d* was the thickness of the active layer, and *V* was the effective voltage $V–V_{bi}$. The hole mobility can be fit from the log *J–V* curve.

AFM and TEM Characterization: Tapping-mode AFM was acquired with an Agilent-5400 scanning probe microscope using a Nanodrive controller with MikroMasch NSC-15 AFM tips and resonant frequencies of ≈300 kHz. TEM was performed with a FEI Tecnai T20 (LaB_6, 200 kV). Without the electrode deposition, the active layer was placed onto a copper grid after dissolving the PEDOT:PSS in water. Samples were dried at room temperature.

GIWAXS Measurements: Grazing incidence X-ray scattering characterization of the thin films was performed at the Advanced Light Source (ALS) on beam 7.3.3.[63] The 10 KeV X-ray beam was incident at a grazing angle of 0.10°–0.15°, which optimized the signal-to-background ratio. The data were processed and analyzed using the NIKA software package.

RSoXS Transmission Measurements: RSoXS transmission characterization was carried out at beamline 11.0.1.2 at the ALS.[64] Samples were prepared on a PEDOT:PSS modified Si substrate, and then transferred to a 1.5 mm × 1.5 mm, 100 nm thick Si_3N_4 membrane supported by a 5 mm × 5 mm, 200 μm thick Si frame (Norcada Inc.). 2D scattering patterns were obtained on an in-vacuum CCD camera (Princeton Instrument PI-MTE).

Time-Resolved Photoluminescence (TRPL) Characterization: A Ti:Sapphire laser (Spectra-Physics, Tsunami) at 800 nm and repetition rate 81 MHz with pulse duration of 100 fs was used as an excitation source. Frequency-doubled light (400 nm, generated by Photop Technologies, Tripler TP-2000B) was used for excitation. PL was collected by using two 1 in. quartz plano-convex lenses of 50 mm focal length and focused on the input slit of a spectrograph (Chromex). The output of the spectrograph was sent into the streak camera (Hamamatsu

C6860) with a slit width of 20 μm. After background correction of the measured PL images, the shading and spectral sensitivity correction of the fluorescence spectrometer was performed by using a calibrated reference light source (Ocean Optics, LS-1-CAL). All samples were kept in N_2 atmosphere, and measured at room temperature. Efforts were taken to keep the same alignment of the experimental set-ups for all the samples studied.

FTPS-EQE Characterization: FTPS-EQE spectra were measured by using a Vertex 70 from Bruker optics with a QTH lamp, quartz beamsplitter, and external detector option. A low noise current amplifier (SR570) was used to amplify the photocurrent produced upon illumination of PSCs with light modulated by the FTIR. The output voltage of the current amplifier was fed back into the external detector port of the FTIR to collect the photocurrent spectrum.

Supporting Information

Supporting Information is available from the Wiley Online Library or from the author.

Acknowledgements

We thank the Swedish Research Council, the Swedish Research Council Formas, the Swedish Energy Agency, Chalmers Area of Advance Energy and Materials Science, and the EU projects SUNFLOWER-"SUstainable Novel FLexible Organic Watts Efficiently Reliable" (FP7-ICT-2011-7, Grant No.: 287594) for financial support. A.Y. acknowledges the Knut and Alice Wallenberg and Crafoord foundations. O.I. thanks the Knut and Alice Wallenberg foundation for a Wallenberg Scholar grant. E.W. acknowledges the program for the Excellent Doctoral Dissertations of Guangdong Province (ybzzxm201114). C.W. and Y.X. thank the China Scholarship Council for a stipend. W.M. thanks the support by National Natural Science Foundation of China (21504066 and 21534003). X-ray data were acquired at beamlines 7.3.3 and 11.0.1.2 at the Advanced Light Source, which is supported by the Director, Office of Science, Office of Basic Energy Sciences of the U.S. Department of Energy under Contract No. DE-AC02-05CH11231.

Received: January 23, 2016
Revised: May 3, 2016
Published online: June 30, 2016

[1] J. Zhao, Y. Li, G. Yang, K. Jiang, H. Lin, H. Ade, W. Ma, H. Yan, *Nat. Energy* **2016**, *1*, 15027.
[2] M. A. Green, K. Emery, Y. Hishikawa, W. Warta, E. D. Dunlop, *Prog. Photovolt: Res. Appl.* **2015**, *23*, 805.
[3] M. Wang, H. Wang, T. Yokoyama, X. Liu, Y. Huang, Y. Zhang, T.-Q. Nguyen, S. Aramaki, G. C. Bazan, *J. Am. Chem. Soc.* **2014**, *136*, 12576.
[4] W. Li, K. H. Hendriks, A. Furlan, M. M. Wienk, R. A. J. Janssen, *J. Am. Chem. Soc.* **2015**, *137*, 2231.
[5] K. Gao, L. Li, T. Lai, L. Xiao, Y. Huang, F. Huang, J. Peng, Y. Cao, F. Liu, T. P. Russell, R. A. J. Janssen, X. Peng, *J. Am. Chem. Soc.* **2015**, *137*, 7282.
[6] D. Veldman, S. C. J. Meskers, R. A. J. Janssen, *Adv. Funct. Mater.* **2009**, *19*, 1939.
[7] C. Deibel, T. Strobel, V. Dyakonov, *Adv. Mater.* **2010**, *22*, 4097.
[8] Y. Liu, J. Zhao, Z. Li, C. Mu, W. Ma, H. Hu, K. Jiang, H. Lin, H. Ade, H. Yan, *Nat. Commun.* **2014**, *5*, 5293.
[9] Z. He, B. Xiao, F. Liu, H. Wu, Y. Yang, S. Xiao, C. Wang, T. P. Russell, Y. Cao, *Nat. Photonics* **2015**, *9*, 174.
[10] V. Vohra, K. Kawashima, T. Kakara, T. Koganezawa, I. Osaka, K. Takimiya, H. Murata, *Nat. Photonics* **2015**, *9*, 403.
[11] H. Zhou, Q. Chen, G. Li, S. Luo, T.-b. Song, H.-S. Duan, Z. Hong, J. You, Y. Liu, Y. Yang, *Science* **2014**, *345*, 542.
[12] N. J. Jeon, J. H. Noh, W. S. Yang, Y. C. Kim, S. Ryu, J. Seo, S. I. Seok, *Nature* **2015**, *517*, 476.
[13] P. K. Nayak, D. Cahen, *Adv. Mater.* **2014**, *26*, 1622.
[14] X. Xu, C. Wang, O. Bäcke, D. I. James, K. Bini, E. Olsson, M. R. Andersson, M. Fahlman, E. Wang, *Polym. Chem.* **2015**, *6*, 4624.
[15] K. Kawashima, Y. Tamai, H. Ohkita, I. Osaka, K. Takimiya, *Nat. Commun.* **2015**, *6*, 10085.
[16] Y.-X. Xu, C.-C. Chueh, H.-L. Yip, F.-Z. Ding, Y.-X. Li, C.-Z. Li, X. Li, W.-C. Chen, A. K. Y. Jen, *Adv. Mater.* **2012**, *24*, 6356.
[17] X. Xu, Z. Li, O. Backe, K. Bini, D. I. James, E. Olsson, M. R. Andersson, E. Wang, *J. Mater. Chem. A* **2014**, *2*, 18988.
[18] H. Li, S. Sun, S. Mhaisalkar, M. T. Zin, Y. M. Lam, A. C. Grimsdale, *J. Mater. Chem. A* **2014**, *2*, 17925.
[19] C. B. Nielsen, R. S. Ashraf, N. D. Treat, B. C. Schroeder, J. E. Donaghey, A. J. P. White, N. Stingelin, I. McCulloch, *Adv. Mater.* **2015**, *27*, 948.
[20] N. J. Turro, V. Ramamurthy, J. C. Scaiano, *Modern Molecular Photochemistry of Organic Molecules*, University Science Books, **2010**.
[21] S. S. Sun, L. R. Dalton, *Introduction to Organic Electronic and Optoelectronic Materials and Devices*, Taylor & Francis, **2008**.
[22] D. Mühlbacher, H. Neugebauer, A. Cravino, N. S. Sariciftci, *Synth. Met.* **2003**, *137*, 1361.
[23] M. C. Scharber, D. Mühlbacher, M. Koppe, P. Denk, C. Waldauf, A. J. Heeger, C. J. Brabec, *Adv. Mater.* **2006**, *18*, 789.
[24] J. J. Intemann, K. Yao, Y.-X. Li, H.-L. Yip, Y.-X. Xu, P.-W. Liang, C.-C. Chueh, F.-Z. Ding, X. Yang, X. Li, Y. Chen, A. K. Y. Jen, *Adv. Funct. Mater.* **2014**, *24*, 1465.
[25] X. Xu, P. Cai, Y. Lu, N. S. Choon, J. Chen, B. S. Ong, X. Hu, *Macromol. Rapid Commun.* **2013**, *34*, 681.
[26] E. Wang, L. Hou, Z. Wang, Z. Ma, S. Hellström, W. Zhuang, F. Zhang, O. Inganäs, M. R. Andersson, *Macromolecules* **2011**, *44*, 2067.
[27] E. Wang, J. Bergqvist, K. Vandewal, Z. Ma, L. Hou, A. Lundin, S. Himmelberger, A. Salleo, C. Müller, O. Inganäs, F. Zhang, M. R. Andersson, *Adv. Energy Mater.* **2013**, *3*, 806.
[28] C. Cabanetos, A. El Labban, J. A. Bartelt, J. D. Douglas, W. R. Mateker, J. M. J. Fréchet, M. D. McGehee, P. M. Beaujuge, *J. Am. Chem. Soc.* **2013**, *135*, 4656.
[29] S. Mukherjee, C. M. Proctor, J. R. Tumbleston, G. C. Bazan, T.-Q. Nguyen, H. Ade, *Adv. Mater.* **2015**, *27*, 1105.
[30] W. Ma, J. R. Tumbleston, L. Ye, C. Wang, J. Hou, H. Ade, *Adv. Mater.* **2014**, *26*, 4234.
[31] W. Chen, T. Xu, F. He, W. Wang, C. Wang, J. Strzalka, Y. Liu, J. Wen, D. J. Miller, J. Chen, K. Hong, L. Yu, S. B. Darling, *Nano Lett.* **2011**, *11*, 3707.
[32] D.-M. Smilgies, *J. Appl. Crystallogr.* **2013**, *46*, 286.
[33] W. Ma, L. Ye, S. Zhang, J. Hou, H. Ade, *J. Mater. Chem. C* **2013**, *1*, 5023.
[34] W. Ma, J. R. Tumbleston, M. Wang, E. Gann, F. Huang, H. Ade, *Adv. Energy Mater.* **2013**, *3*, 864.
[35] L.-M. Chen, Z. Hong, G. Li, Y. Yang, *Adv. Mater.* **2009**, *21*, 1434.
[36] M. Tong, N. E. Coates, D. Moses, A. J. Heeger, S. Beaupré, M. Leclerc, *Phys. Rev. B* **2010**, *81*, 125210.
[37] J. K. J. van Duren, X. Yang, J. Loos, C. W. T. Bulle-Lieuwma, A. B. Sieval, J. C. Hummelen, R. A. J. Janssen, *Adv. Funct. Mater.* **2004**, *14*, 425.
[38] Y. Zhou, K. Tvingstedt, F. Zhang, C. Du, W.-X. Ni, M. R. Andersson, O. Inganäs, *Adv. Funct. Mater.* **2009**, *19*, 3293.
[39] K. Tvingstedt, K. Vandewal, F. Zhang, O. Inganäs, *J. Phys. Chem. C* **2010**, *114*, 21824.
[40] T. Offermans, P. A. van Hal, S. C. J. Meskers, M. M. Koetse, R. A. J. Janssen, *Phys. Rev. B* **2005**, *72*, 045213.

[41] M. A. Loi, S. Toffanin, M. Muccini, M. Forster, U. Scherf, M. Scharber, *Adv. Funct. Mater.* **2007**, *17*, 2111.
[42] Z. Ma, W. Sun, S. Himmelberger, K. Vandewal, Z. Tang, J. Bergqvist, A. Salleo, J. W. Andreasen, O. Inganäs, M. R. Andersson, C. Müller, F. Zhang, E. Wang, *Energy Environ. Sci.* **2014**, *7*, 361.
[43] W. Zhang, R. Hu, D. Li, M.-M. Huo, X.-C. Ai, J.-P. Zhang, *J. Phys. Chem. C* **2012**, *116*, 4298.
[44] J. Guo, H. Ohkita, H. Benten, S. Ito, *J. Am. Chem. Soc.* **2009**, *131*, 16869.
[45] I. A. Howard, R. Mauer, M. Meister, F. Laquai, *J. Am. Chem. Soc.* **2010**, *132*, 14866.
[46] S. De, T. Pascher, M. Maiti, K. G. Jespersen, T. Kesti, F. Zhang, O. Inganäs, A. Yartsev, V. Sundström, *J. Am. Chem. Soc.* **2007**, *129*, 8466.
[47] S. K. Pal, T. Kesti, M. Maiti, F. Zhang, O. Inganäs, S. Hellström, M. R. Andersson, F. Oswald, F. Langa, T. Österman, T. Pascher, A. Yartsev, V. Sundström, *J. Am. Chem. Soc.* **2010**, *132*, 12440.
[48] A. C. Morteani, R. H. Friend, C. Silva, *J. Chem. Phys.* **2005**, *122*, 244906.
[49] K. Vandewal, A. Gadisa, W. D. Oosterbaan, S. Bertho, F. Banishoeib, I. Van Severen, L. Lutsen, T. J. Cleij, D. Vanderzande, J. V. Manca, *Adv. Funct. Mater.* **2008**, *18*, 2064.
[50] K. Vandewal, K. Tvingstedt, A. Gadisa, O. Inganäs, J. V. Manca, *Nat. Mater.* **2009**, *8*, 904.
[51] K. Vandewal, K. Tvingstedt, A. Gadisa, O. Inganäs, J. V. Manca, *Phys. Rev. B* **2010**, *81*, 125204.
[52] J. Yao, T. Kirchartz, M. S. Vezie, M. A. Faist, W. Gong, Z. He, H. Wu, J. Troughton, T. Watson, D. Bryant, J. Nelson, *Phys. Rev. Appl.* **2015**, *4*, 014020.
[53] M. C. Scharber, N. S. Sariciftci, *Prog. Polym. Sci.* **2013**, *38*, 1929.
[54] J. Yuan, Z. Zhai, H. Dong, J. Li, Z. Jiang, Y. Li, W. Ma, *Adv. Funct. Mater.* **2013**, *23*, 885.
[55] J. Warnan, A. El Labban, C. Cabanetos, E. T. Hoke, P. K. Shukla, C. Risko, J.-L. Brédas, M. D. McGehee, P. M. Beaujuge, *Chem. Mater.* **2014**, *26*, 2299.
[56] J. Warnan, C. Cabanetos, R. Bude, A. El Labban, L. Li, P. M. Beaujuge, *Chem. Mater.* **2014**, *26*, 2829.
[57] K. H. Hendriks, G. H. L. Heintges, V. S. Gevaerts, M. M. Wienk, R. A. J. Janssen, *Angew. Chem. Int. Ed.* **2013**, *52*, 8341.
[58] L. Dou, W.-H. Chang, J. Gao, C.-C. Chen, J. You, Y. Yang, *Adv. Mater.* **2013**, *25*, 825.
[59] H. Choi, S.-J. Ko, T. Kim, P.-O. Morin, B. Walker, B. H. Lee, M. Leclerc, J. Y. Kim, A. J. Heeger, *Adv. Mater.* **2015**, *27*, 3318.
[60] H. Hu, K. Jiang, G. Yang, J. Liu, Z. Li, H. Lin, Y. Liu, J. Zhao, J. Zhang, F. Huang, Y. Qu, W. Ma, H. Yan, *J. Am. Chem. Soc.* **2015**, *137*, 14149.
[61] K. Tvingstedt, O. Malinkiewicz, A. Baumann, C. Deibel, H. J. Snaith, V. Dyakonov, H. J. Bolink, *Sci. Rep.* **2014**, *4*, 6071.
[62] D. Bi, W. Tress, M. I. Dar, P. Gao, J. Luo, C. Renevier, K. Schenk, A. Abate, F. Giordano, J. P. Correa Baena, J. D. Decoppet, S. M. Zakeeruddin, M. K. Nazeeruddin, M. Gratzel, A. Hagfeldt, *Sci. Adv.* **2016**, *2*, e1501170.
[63] H. Alexander, B. Wim, G. James, S. Eric, G. Eliot, K. Rick, M. Alastair, C. Matthew, R. Bruce, P. Howard, *J. Phys. Conf. Ser.* **2010**, *247*, 012007.
[64] E. Gann, A. T. Young, B. A. Collins, H. Yan, J. Nasiatka, H. A. Padmore, H. Ade, A. Hexemer, C. Wang, *Rev. Sci. Instrum.* **2012**, *83*, 045110.